INTERNATIONAL JOURNAL FOR NUMERICAL METHODS IN FLUIDS, VOL. 25, 1107–1117 (1997)

APPLICATION OF FOURTH-ORDER DIFFERENCE METHOD TO PREDICTION OF TURBULENCE CONTROL IN TWO-DIMENSIONAL CHANNEL WITH SURFACE ROUGHNESS

HIROSHI TOKUNAGA* AND AKIRA YAMAUCHI

Department of Mechanical and System Engineering, Kyoto Institute of Technology, Matsugasaki, Sakyo-ku, Kyoto 606, Japan

SUMMARY

The fourth-order finite difference method is combined with the vorticity–streamfunction formulation in generalized co-ordinates. Direct numerical simulations are performed for channel flows with and without surface roughness at a Reynolds number of 10^4. The present results are in good agreement with those of the pseudospectral method with respect to the flow in a smooth channel. It is shown that the present method predicts well the precise change in the flow with the channel length and roughness height. The turbulence is generally weakened by the roughness. Laminarization is also accomplished under the appropriate condition. © 1977 John Wiley & Sons, Ltd.

Int. J. Numer. Meth. Fluids, **25**: 1107–1117 (1997)

No. of Figures: 13. No. of Tables: 0. No. of References: 9.

KEY WORDS: fourth-order finite difference method; vorticity–streamfunction formulation; general geometry; turbulence control; drag reduction; roughness

1. INTRODUCTION

Drag reduction is an important problem and several different means of achieving it, such as riblets, polymer additions and compliant walls, have been investigated.[1,2] Recently, Manuilovich[3] proposed laminarization of the boundary layer by surface roughness. It is shown theoretically that the Tollmien–Schlichting wave (T–S wave) cancels over the appropriate surface roughness. This suggests that the drag reduction is produced by two-dimensional means. On the other hand, Liu *et al.*[4] conducted numerical simulations of the flow in a rough channel by the multilevel method and showed that the T–S wave is strengthened by the roughness. However, in these investigations the disturbance is assumed to be small and linearization of the Navier–Stokes equation is applied. In the present paper we conduct numerical simulations of turbulent flows in smooth and rough channels, using the Navier–Stokes equation. It is well known that turbulent flow is governed by the complex temporal and spatial structure and therefore numerical results depend significantly on the computational method. For this we use the fourth-order-accurate difference method[5,6] combined with the vorticity–streamfunction formulation.[7,8] In a smooth channel flow we compare the results with those of Jiménez[9] using the pseudospectral method. In a rough channel flow we study the drag reduction and laminarization of the flow.

*Correspondence to: H. Tokunaga, Department of Mechanical and System Engineering, Kyoto Institute of Technology, Matsugasaki, Sakyo-ku, Kyoto 606, Japan.

CCC 0271–2091/97/101107–11 $17.50

Received October 1995
Revised November 1996

2. GOVERNING EQUATIONS AND COMPUTATIONAL METHODS

2.1. Vorticity–streamfunction formulation

For the computation of channel flow with surface roughness the generalized co-ordinates

$$x = x(\xi, \eta), \qquad y = y(\xi, \eta) \tag{1}$$

are adopted. In order to satisfy the equation of continuity rigorously, we use the vorticity–streamfunction formulation. Then the governing equations consist of the vorticity transport equation and the Poisson equation for the streamfunction, i.e.

$$\frac{\partial \omega}{\partial t} + \frac{1}{J}\frac{\partial(\omega, \psi)}{\partial(\xi, \eta)} = \frac{1}{Re}\Delta\omega, \tag{2}$$

$$\Delta\psi = -\omega, \tag{3}$$

where the Laplacian is represented by

$$\Delta = \alpha\frac{\partial^2}{\partial\xi^2} - 2\beta\frac{\partial^2}{\partial\xi\partial\eta} + \gamma\frac{\partial^2}{\partial\eta^2} + \sigma\frac{\partial}{\partial\xi} + \tau\frac{\partial}{\partial\eta}. \tag{4}$$

The metrics are expressed as

$$\begin{aligned}
&\alpha = \left(\frac{\partial x}{\partial\eta}\right)^2 + \left(\frac{\partial y}{\partial\eta}\right)^2, \qquad \beta = \frac{\partial x}{\partial\xi}\frac{\partial x}{\partial\eta} + \frac{\partial y}{\partial\xi}\frac{\partial y}{\partial\eta}, \qquad \gamma = \left(\frac{\partial x}{\partial\xi}\right)^2 + \left(\frac{\partial y}{\partial\xi}\right)^2,\\
&\sigma = -\frac{1}{J}\left(D_x\frac{\partial y}{\partial\eta} - D_y\frac{\partial x}{\partial\eta}\right), \qquad \tau = \frac{1}{J}\left(D_x\frac{\partial y}{\partial\xi} - D_y\frac{\partial x}{\partial\xi}\right),\\
&D_x = \alpha\frac{\partial^2 x}{\partial\xi^2} - 2\beta\frac{\partial^2 x}{\partial\xi\partial\eta} + \gamma\frac{\partial^2 x}{\partial\eta^2}, \qquad D_y = \alpha\frac{\partial^2 y}{\partial\xi^2} - 2\beta\frac{\partial^2 y}{\partial\xi\partial\eta} + \gamma\frac{\partial^2 y}{\partial\eta^2}
\end{aligned} \tag{5}$$

and J denotes the Jacobian. The velocity components u and v

$$u = \frac{1}{J}\frac{\partial(x, \psi)}{\partial(\xi, \eta)}, \qquad v = \frac{1}{J}\frac{\partial(y, \psi)}{\partial(\xi, \eta)}. \tag{6}$$

These equations are non-dimensionalized with the channel half-width δ and the centre velocity of the Poiseuille flow, U_c. Re denotes the Reynolds number.

2.2. Boundary conditions

The computational domain is depicted in Figure 1, where L_x represents the channel length. The surface roughness is given by[4]

$$r(x) = \kappa\ \mathrm{sech}^2[\sqrt{2}(x - x_p)], \tag{7}$$

where κ denotes the roughness height and x_p the location of the roughness. In the present study, κ is chosen as 0·02 or 0·06, and $x_p = \pi$.

The streamfunction takes constant values of $\pm\frac{2}{3}$ at the upper and lower walls, respectively. The boundary vorticity is calculated from the following definition, where the non-slip condition is applied at the channel wall:

$$\omega = -\frac{1}{J}\left(\frac{\partial y}{\partial\xi}\frac{\partial v}{\partial\eta} + \frac{\partial x}{\partial\xi}\frac{\partial u}{\partial\eta}\right). \tag{8}$$

On the other hand, a periodic boundary condition is imposed in the streamwise direction.

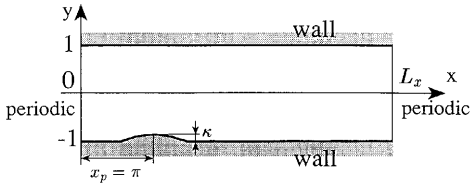

Figure 1. Computational domain

2.3. Computational Grid

In order to calculate the channel flow with surface roughness, the computational grid is given as

$$\begin{aligned} x_i &= \frac{\xi_i}{I-1}L_x \quad (\xi_i = i-1), \\ y_{ij} &= (1-\tfrac{1}{2}r_i)\tanh\left[\left(-1+\frac{2\eta_j}{J-1}\right)\tanh^{-1}\alpha\right]/\alpha + \tfrac{1}{2}r_i, \quad (\eta_j = j-1), \end{aligned} \tag{9}$$

where r_i denotes the roughness height at $x = x_i$, the parameter $\alpha = 0{\cdot}9$, and I and J represent the total grid numbers in the ξ- and η-direction respectively.

2.4. Fourth-order difference method

In order to solve accurately the unsteady flow with the complex spatial structure, we use the fourth-order-accurate centred difference method without numerical dissipation. In the present method the spatial discretization and time integration are treated separately. For example, the first and second derivatives of ω with respect to ξ are differenced as

$$\begin{aligned} \left.\frac{\partial\omega}{\partial\xi}\right|_{ij} &= \frac{-\omega_{i+2,j} + 8\omega_{i+1,j} - 8\omega_{i-1,j} + \omega_{i-2,j}}{12\Delta\xi} \\ \left.\frac{\partial^2\omega}{\partial\xi^2}\right|_{ij} &= \frac{-\omega_{i+2,j} + 16\omega_{i+1,j} - 30\omega_{i,j} + 16\omega_{i-1,j} - \omega_{i-2,j}}{12\Delta\xi^2} \end{aligned} \tag{10}$$

where $\Delta\xi$ denotes the grid spacing in the ξ-direction. The derivatives for η and the cross-derivative are also differenced in the same manner. Then the vorticity transport equation is reduced to a set of ordinary differential equations (ODEs) with respect to the vorticity values at all inner grid points:

$$\frac{\mathrm{d}\vec{\omega}}{\mathrm{d}t} = \vec{F}(\vec{\omega}), \tag{11}$$

$$\vec{\omega} = (\omega_{2,2}, \omega_{3,2}, \ldots, \omega_{I-1,J-1})^{\mathrm{T}}, \tag{12}$$

The set of ODEs is integrated with the fourth-order Runge–Kutta–Gill method.

The same spatial discretization is adopted for the Poisson equation. The point Jacobi method is used as the relaxation in the ξ-direction for vectorizing the computational code, since the Fujitsu FACOM VP-2600 and VPP-500 used in the present computations have a long-pipeline architecture and approximately 500 processors are aligned. The SOR method, however, is applied in the η-direction for accelerating the convergence even though the fourth-order difference method is being used. The acceleration factor is chosen appropriately for getting the optimum convergence rate. As a result of several trial computations it is found that a large number of relaxation sweep are necessary,

since the flow field changes drastically in time. If the relaxation sweep is insufficient, the turbulence weakens significantly.

3. COMPUTATION OF TURBULENT FLOW IN SMOOTH CHANNEL

The flow in a smooth channel has already been computed for a number of conditions.[8] In the present paper we describe only the computational results at $Re = 10^4$ for comparison with the flow in a rough channel.

3.1. Computation of flow in period doubling

The channel flow at $Re = 10^4$ is computed for $L_x = 2\pi$ with a 129×97 grid. Figure 2 depicts the time evolution of the wall shear stress Ω, which shows that the flow is in a state of period doubling. The time-averaged wall shear stress equals 3·551, the maximum amplitude of the oscillation 0·053 and the minimum amplitude 0·040, which are in good agreement with Jiménez's results, namely 3·547, 0·053 and 0·038 respectively.

The vorticity isolines are shown in Figure 3, where two periodic regions are depicted. It is shown that the vortex elongates extremely and tears, while the torn vortex approaches the wall. The agreement of the present result with Jiménez's computation is quite good.

3.2. Computation of two-dimensional turbulence in long channel

Here we deal with the computation of a chaotic flow in a channel. The channel length is chosen as 8π, the Reynolds number 10^4, the grid 615×121 and the time spacing $\Delta t = 0{\cdot}01$. Basically, the initial streamfunction is constructed with the preceding solution $\psi_{2\pi}(x, y, t_0)$ with periodicity 2π, where t_0 represents an appropriate time. However, in order to change the periodic length to 8π, the streamfunction is actually given as

$$\psi(x, y, 0) = [1 + 0{\cdot}05 \cos(x/4)]\psi_{2\pi}(x, y, t_0). \tag{13}$$

Figure 4 depicts the vorticity isolines from $t = 330$ to 340. The vortex rolls up from the wall, elongates and tears. However, the torn vortex approaches the wall and merges into another rolled-up

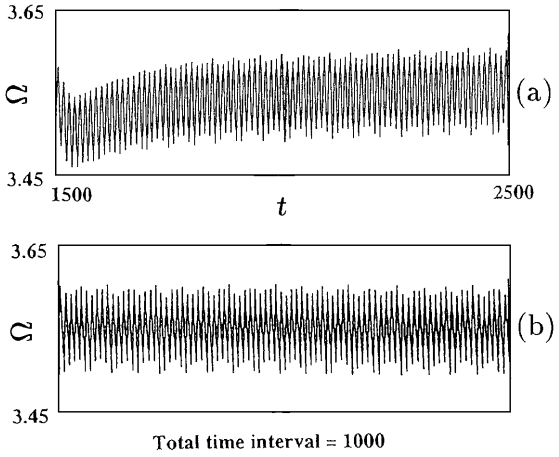

Figure 2. Time evolution of wall shear stress in smooth channel at $L_x = 2\pi$: (a) present results; (b) Jiménez's result

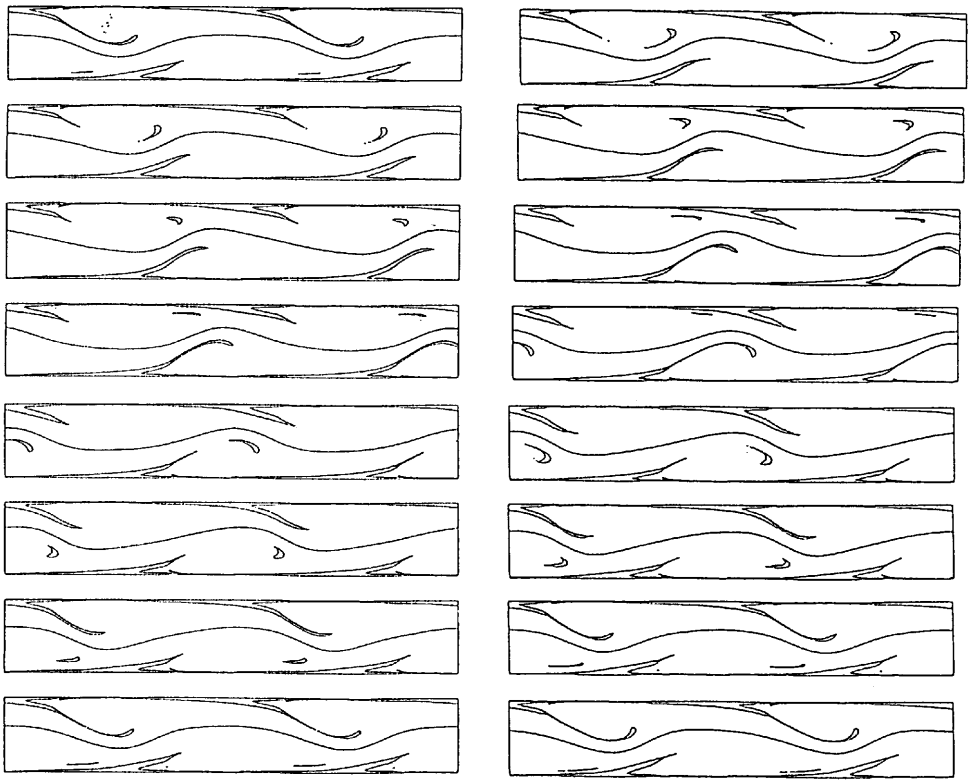

(a) (b)

Figure 3. Vorticity isolines in smooth channel: (a) present results; (b) Jiménez's result ($\omega = 0, \pm 1{\cdot}5$)

vortex, in the present case. After a short period the merging vortex separates from the rolled-up vortex, approaches a newly rolled-up vortex and disturbs the vortex elongation. Therefore the vortex interactions in four regions of length 2π are not independent of each other, so that irregularity arises and the flow becomes chaotic.

The time evolution of the wall shear stress is plotted for the upper wall until $t = 350$ in Figure 5. The period-doubling structure is seen at the initial stage and then the chaotic structure appears. The magnitude of the wall shear stress increases by 15% compared with the result in the short channel.

4. COMPUTATION OF TURBULENT FLOW IN CHANNEL WITH ROUGHNESS

4.1. Computation of flow in short rough channel

The first computation of channel flow with surface roughness is carried out for $L_x = 2\pi$ and $\kappa = 0{\cdot}06$. Under this condition the flow is in a state of period doubling if the surface roughness is not imposed, as described in the preceding section.

A 128×85 grid was necessary to resolve the flow. Figure 6 depicts the time evolution of the wall shear stress at the lower and upper walls from $t = 1000$ to 1600. It is confirmed that the flow is in a state of period doubling as in the smooth channel. However, the mean wall shear stress of 3·22 on the

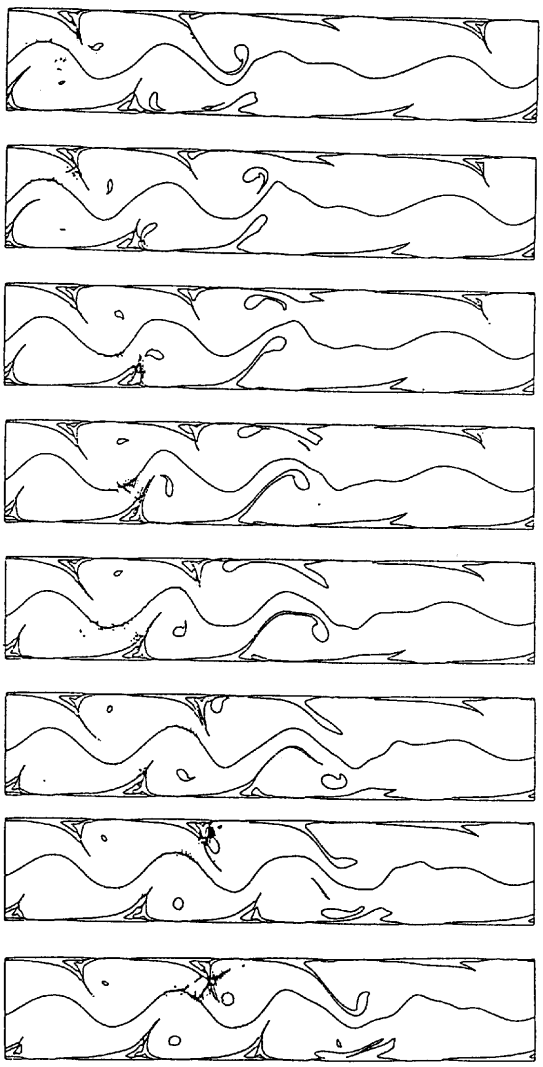

Figure 4. Vorticity isolines of turbulence in smooth channel at $L_x = 8\pi$ ($\omega = 0, \pm 1{\cdot}5$)

lower wall is smaller than that of 3·65 on the upper wall and the value of 3·55 in the smooth channel. The vorticity isolines are depicted at $t = 1600$ in Figure 7. The same rolled-up vortex is created from the upper wall as in the smooth channel. However, significant interaction between the rolled-up vortex and the rough wall is found on the lower wall. As a result of this interaction the rolled-up vortex is weakened.

4.2. Computation of turbulent flow in long channel with surface roughness

In order to investigate the effect of surface roughness on two-dimensional turbulence, a numerical simulation is conducted for a flow with roughness height $\kappa = 0{\cdot}02$ and channel length 8π. A 1024×85 grid is necessary in the present computation.

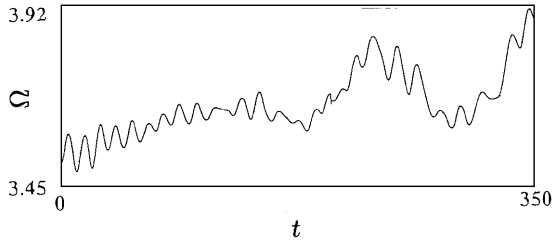

Figure 5. Time evolution of wall shear stress in smooth channel at $L_x = 8\pi$

Figures 8 and 9 show the vorticity isolines and streamlines respectively in the fully developed state. It is seen that the rolled-up vortex is weakened by the surface roughness and recovers its strength soon after passing the roughness. The separation bubbles in Figure 9 show the same tendency as the vorticity structure. The time evolution of the wall shear stress is depicted from $t = 260$ to 400 in Figure 10. The time-averaged values are 3·2 and 3·5 on the lower and upper walls, respectively, which are significantly smaller, than those of the smooth channel. Therefore it is shown that drag reduction is achieved by the roughness.

4.3. Computation of turbulent flow in medium channel with surface roughness

In order to study the possibility of laminarization of the flow by the surface roughness, a computation is carried out for a medium channel with $L_x = 4\pi$ and $\kappa = 0{\cdot}06$. The initial condition is given by fitting the velocity field of plane Poiseuille flow to the channel with surface roughness. In this case a 512×85 grid is necessary. The history of the x-directional velocity is depicted at the point $x = 0$ and the fifth grid point in the η-direction in Figure 11. A strong disturbance is first generated, which then changes to a small oscillation. The wall shear stress on the lower and upper walls is shown

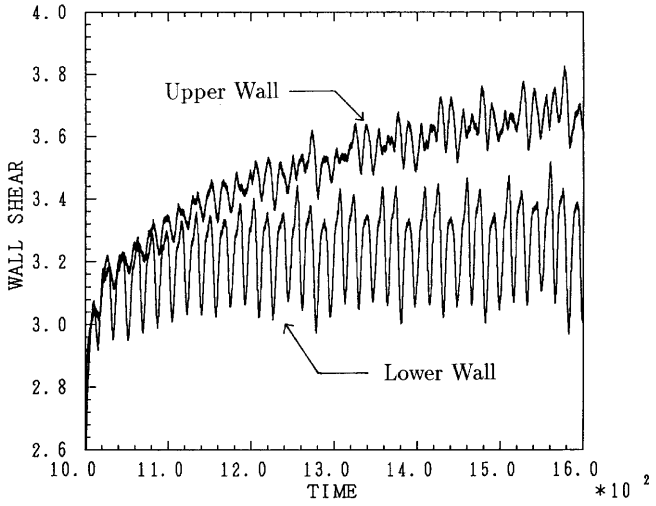

Figure 6. Time evolution of wall shear stress in rough channel at $L_x = 2\pi$ and $\kappa = 0{\cdot}06$

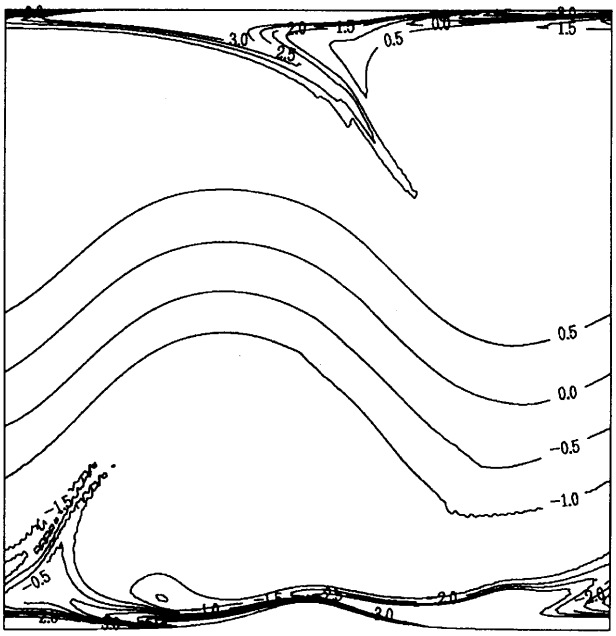

Figure 7. Vorticty isolines in rough channel at $L_x = 2\pi$, $\kappa = 0{\cdot}06$ and $t = 1600$

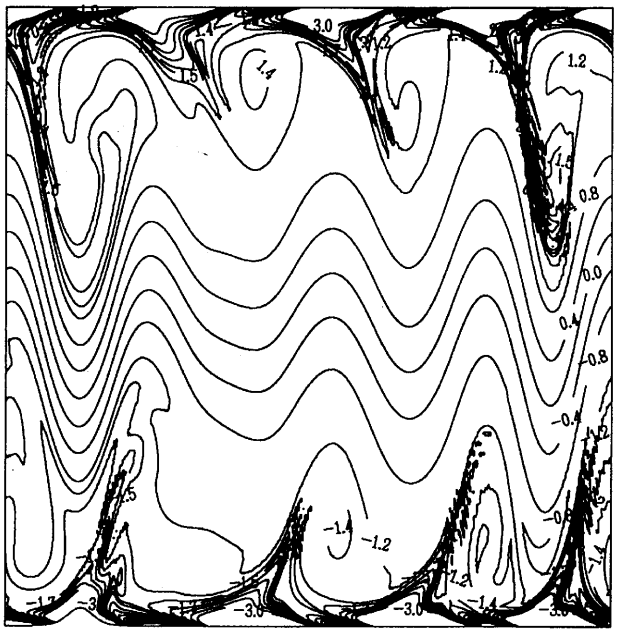

Figure 8. Vorticity isolines in rough channel at $L_x = 8\pi$ and $\kappa = 0{\cdot}02$

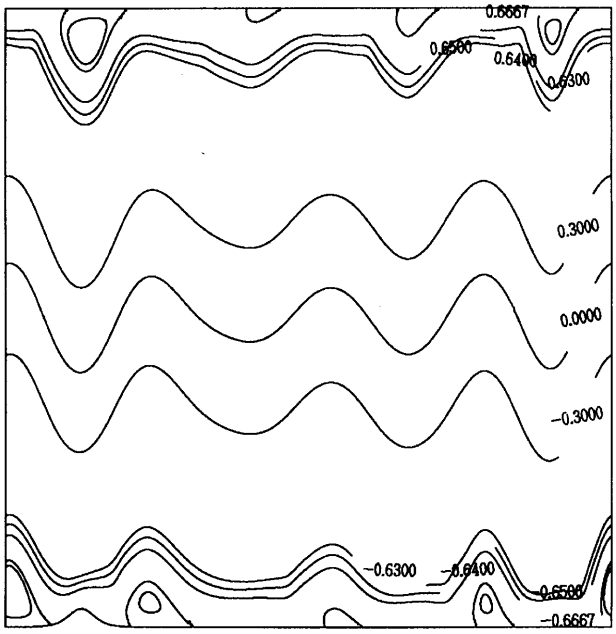

Figure 9. Streamlines in rough channel at $L_x = 8\pi$ and $\kappa = 0{\cdot}02$

in Figure 12, where complete laminarization is found. Figure 13 depicts the vorticity contours at $t = 360$, which show that the disturbance is trapped on the roughness and eliminated.

5. CONCLUSIONS

The fourth-order difference method is implemented with the vorticity–streamfunction formulation in a generalized co-ordinate system and numerical simulations are conducted for flows in channels with and without surface roughness. From the results the following conclusions are obtained.

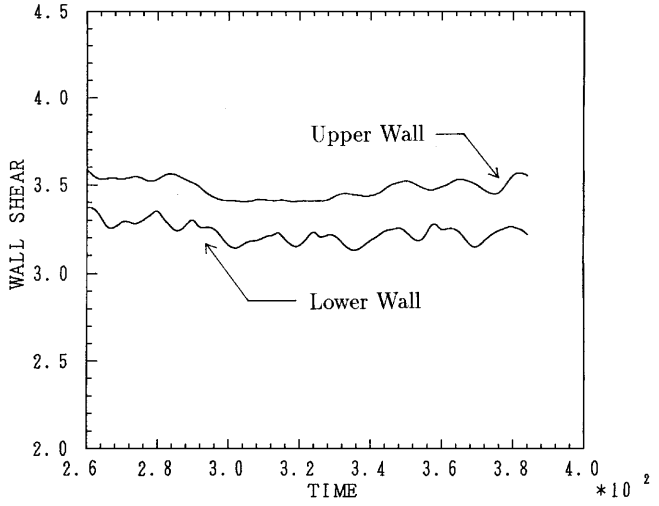

Figure 10. Time evolution of wall shear stress in rough channel at $L_x = 8\pi$ and $\kappa = 0{\cdot}02$

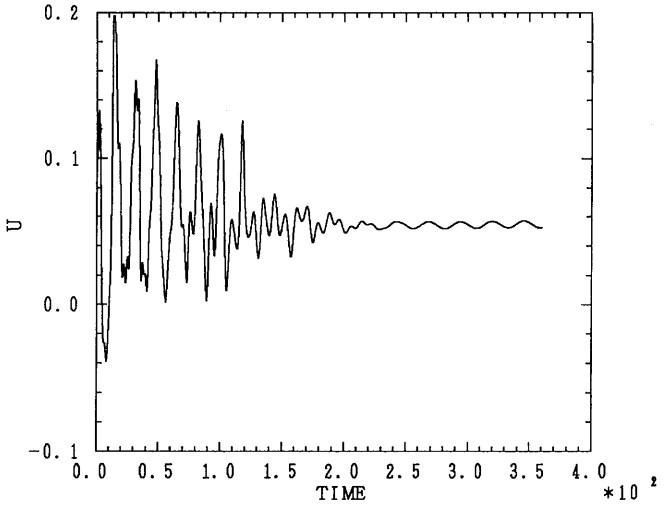

Figure 11. Time history of x-directional velocity near wall in rough channel at $L_x = 4\pi$ and $\kappa = 0{\cdot}06$

1. Good agreement with Jiménez's result is obtained with respect to the flow in a smooth channel, in which period-doubling is realized.
2. In a long channel, chaotic flow is produced which consists of ejection, tearing, sweeping and merging of vortices.
3. It is shown that the surface roughness has the effect of weakening the turbulence. Laminarization of the flow is accomplished under the appropriate condition.

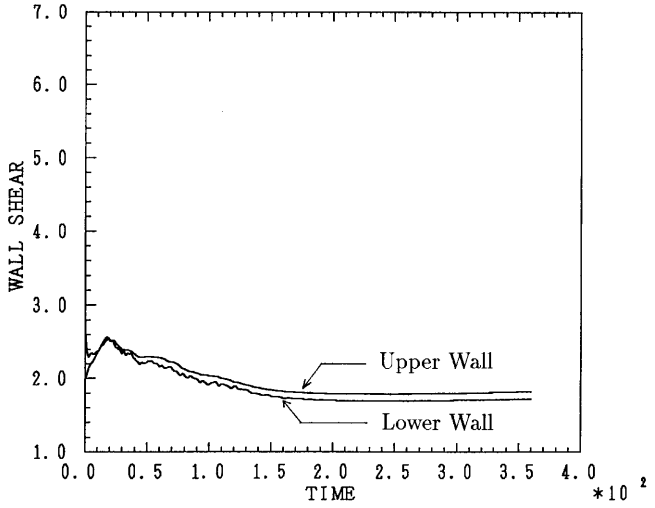

Figure 12. Time evolution of wall shear stress in rough channel at $L_x = 4\pi$ and $\kappa = 0{\cdot}06$

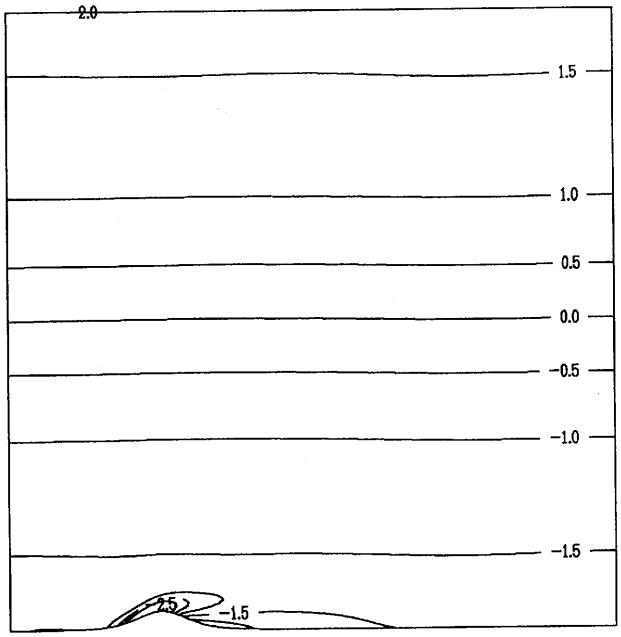

Figure 13. Vorticity isolines in rough channel at $L_x = 4\pi$ and $\kappa = 0{\cdot}06$

REFERENCES

1. D. M. Bushnell and C. B. McGinley, 'Turbulence control in wall flows', *Ann. Rev. Fluid Mech.*, **21**, 1–20 (1989).
2. H. Choi, P. Moin and J. Kim, 'Active turbulence control for drag reduction in wall-bounded flows', *J. Fluid Mech.*, **262**, 75–110 (1994).
3. S. V. Manuilovich, 'On new methods for boundary-layer flow laminarization', *Theor. Comput. Fluid Dyn.*, **6**, 31–47 (1994).
4. Z. Liu, C. Liu and S. McCormick, 'Multilevel methods for temporal and spatial flow transition simulation in a rough channel', *Int. j. num. methods fluids*, **19**, 23–40 (1994).
5. H. Tokunaga, K. Ichinose and N. Satofuka, 'Numerical simulations of transition to turbulence using higher order method of lines', *Lect. Notes Phys.*, **371**, 183–185 (1990).
6. H. Tokunaga, 'LES of transition in channel flow using vorticity–vector potential formulation', *Proc. 1st Asian Computational Fluid Dynamics Conf.*, eds., W.H. Hui, Y.K. Kwok and J.R. Chashnov, Hong Kong University of Science & Technology, 1995, pp. 767–772.
7. H. Tokunaga, 'Numerical simulations using vorticty–vector potential formulation', *Annual Research Briefs, Center for Turbulence Research*, Stanford University/NASA Ames, 1992, pp. 175–184.
8. H. Tokunaga and A. Yamauchi, 'Numerical simulations of turbulence control in two-dimensional channel flow with surface roughness', in C. Taylor and P. Durbetaki (eds), *Proc. Ninth Int. Conf. on Numerical Methods Laminar and Turbulent Flow*, Pineridge, Swansea, 1995, pp. 1223–1234.
9. J. Jiménez, 'Transition to turbulence in two-dimensional Poiseuille flow', *J. Fluid Mech.*, **218**, 265–297 (1990).

